Nonlinear Analytical Model for Predicting Magnet Loss in Surface-Mounted Permanent-Magnet Motors

Zhaokai Li[1], Xiaoyan Huang[1], *Member IEEE*, Xiaofeng Xu[1], Zhuo Chen[1], Ze Jiang[1], Lijian Wu[1], *Senior Member IEEE*, Tingna Shi[1], *Member IEEE*, and Jian Zhang[1]

[1]Zhejiang Provincial Key Laboratory of Electrical Machine Systems, College of Electrical Engineering, Zhejiang University, Hangzhou, 310027, China

This paper develops a nonlinear analytical model (NAM) for predicting the magnet loss of surface-mounted permanent-magnet motors considering nonlinearity effect and slotting effect. The analytical expression of vector magnetic potential in the permanent-magnet (PM) region is derived from the Hague's equation for slotless air-gap and then it is extended for slotted air-gap based on the conformal mapping method. The PMs, iron nonlinearity and winding current contributing to the eddy current are all represented by equivalent current in the analytical model. The key of the proposed model is to solve the equivalent current of iron nonlinearity from the improved magnetic circuit model (IMCM) of iron region, where the air flux source is proposed to replace the air reluctance. It is found that the iron saturation can decrease the amplitude of flux density and therefore reduce the magnet loss. Based on the NAM, the magnet loss can be obtained with high accuracy and high efficiency, which is a powerful tool for the optimization of magnet loss in the motor design. The effectiveness of the proposed model is verified by the finite element method.

Index Terms—Analytical model, iron saturation, magnet loss, slotting effect.

I. INTRODUCTION

THE EDDY-CURRENT effect plays an important role in the loss analysis of high-speed motors. Researchers have paid much attention to the accurate prediction of eddy-current loss in the recent decades [1]. The finite-element method (FEM) is used to predict magnet loss with acceptable calculation time owing to the rapid development of computer performance. It has been employed in most of the motor design software [2]. However, at the initial design and optimization stage, the analytical models are preferred, which saves large computation resource and provide insights about the magnet loss.

Although the analytical model can efficiently predict the magnet loss of PM motors, it makes much simplification to obtain the analytical expression and therefore lower the calculation accuracy. In [3], the magnetic field of slotless PM motor is analyzed using the analytical model and its magnet loss due to winding current can be predicted accordingly. However, these analytical models cannot be used for slotted PM motor as the slotting effect will significantly increase the magnet loss [4]. To account for slotting effect, either relative permeance model [5] or the complex permeance model [6] can be employed to calculate the magnet loss [7]. However, both models neglect the deformation of magnet for calculating the air permeance function, making their accuracy unsatisfactory.

To further improve the calculation accuracy, either conformal mapping model [8]-[9] or subdomain model [10]-[11] is proposed to calculate the magnet loss. These models show the highest accuracy to predict the magnetic field distribution of surface-mounted permanent-magnet (SPM) motors among the linear analytical models [9]-[11]. Based on these models, the magnet loss is calculated with high accuracy when neglecting iron nonlinearity [12]-[13]. Such simplification can bring in large errors for SPM motors under on-load condition when it suffers from high iron nonlinearity. Hence, it is necessary and important to investigate the nonlinear analytical model and build the relationship between the iron nonlinearity and magnet loss, which is the main contribution of this paper.

The hybrid analytical model which combines the complex permeance model and magnetic circuit model was proposed in [14]-[15] considering both slotting effect and iron nonlinearity. However, this model still ignores the magnet deformation for calculating the complex permeance. In [16]-[17], the conformal mapping combined with magnet circuit model is proposed to consider the magnet deformation, but it neglects the slot leakage in the magnetic circuit model and therefore always underestimates the magnetic field prediction.

In this paper, the NAM is proposed to calculate the magnet loss considering slotting effect and nonlinearity effect. The equivalent current representing PM, winding current and iron nonlinearity is introduced to calculate the vector magnetic potential in the PM region using conformal mapping and Hague's equation. The equivalent current of iron nonlinearity is derived from the IMCM of stator iron, where the air reluctance in the slot and air-gap region is replaced by the air flux source. Based on NAM, the influence of iron nonlinearity on the magnet loss is investigated in the 8-pole/9-slot and 10-pole/12-slot SPM motors. Ultimately, the analysis using FEM is carried out to show its high accuracy and high efficiency.

II. NONLINEAR ANALYTICAL FIELD MODEL

The NAM for predicting the magnetic field in the PM region has the assumptions of negligible end effect, negligible eddy current in the steel lamination, linear property of PM, negligible eddy-current redistribution effect, and resistance limited eddy current in PMs. The iron nonlinearity is represented using the equivalent current in the slot. Therefore, the eddy current and the corresponding magnet loss can be calculated considering iron nonlinearity.

According to Ampere's law, the equivalent nonlinear current located in the slot is expressed as

$$i_{nc} = -\left(V_{nc1} - V_{nc2}\right) \tag{1}$$

where V_{nc1} and V_{nc1} are the magnetic potential between the stator teeth [15]. They can be obtained from the IMCM of stator in Fig. 1.
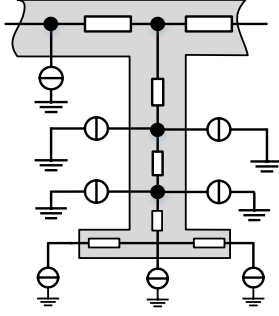

Fig. 1 The schematic view of IMCM for SPM motor.

According to Kirchhoff's Law, the stator IMCM can be solved using

$$f(\mathbf{\Psi_s}) = \mathbf{A_s \Lambda_s A_s^T V} - \mathbf{\Phi_s} = 0 \tag{2}$$

where $\mathbf{\Psi_s}$ and $\mathbf{\Phi_s}$ are the matrix form of magnetic potential and air flux source. $\mathbf{\Lambda_s}$ and $\mathbf{A_s}$ are branch permeance matrix and node incidence matrix in the IMCM.

For PMs with radial magnetization, the equivalent current is uniformly distributed along the edges of PMs in the radial direction. The PM equivalent current is calculated using

$$i_{PM} = \frac{B_r h_m}{\mu_r N_{PM}} \tag{3}$$

where N_{PM} is the number of equivalent current along the edge of PM. B_r, u_r, and h_m are the remanence, permeability and height of PM, respectively.

Then, according to Hague's equation, the magnetic vector potential of PM $A_z(r_{\psi PM}, \alpha_{\psi PM})$ in the annulus produced by the equivalent current $i_c(r_{\psi c}, \alpha_{\psi c})$ is calculated using

$$A_z = \frac{\mu_0 i_c}{2\pi} \left\{ \sum_{k=1}^{+\infty} \ln\left[r_{\psi PM}^2 + r_{\psi c}^2 - 2r_{\psi PM} r_{\psi c} \cos(\alpha_{\psi PM} - \alpha_{\psi c}) \right] \right.$$
$$- \frac{1}{k} \frac{r_{\psi r}^{2k} \left[r_{\psi PM}^k r_{\psi s}^{-k} \left(r_{\psi c}^{2k} r_{\psi r}^{-2k} + 1 \right) + r_{\psi PM}^{-k} r_{\psi s}^k \left(r_{\psi s}^{-2k} r_{\psi c}^{2k} + 1 \right) \right]}{\left(r_{\psi s}^{2k} - r_{\psi r}^{2k} \right)}$$
$$\left. \cos\left[k\left(\alpha_{\psi PM} - \alpha_{\psi c} \right) \right] \right\} \tag{4}$$

where the equivalent current i_c is located at $(r_{\psi c}, \alpha_{\psi c})$ in the annulus [18]. $r_{\psi r}$ and $r_{\psi s}$ are the inner and outer radii of annulus. As the conformal mapping preserves the vector potential value during the transformation, the magnetic vector potential at (r_S, α_S) in the slotted air-gap of real SPM motor is equal to that at (r_ψ, α_ψ) in the annulus.

$$A_z(r_S, \alpha_S) = A_z(r_\psi, \alpha_\psi) \tag{5}$$

where the geometric relationship of the same position between the slotted air-gap (S domain) and annular air-gap (Ψ domain) is built based on the exponential mapping, Schwarz-Christoffel (SC) mapping, and modified logarithmic mapping [8].

$$\psi = r_\psi e^{j\alpha_\psi} = e^{-j\frac{2\pi}{w_r}\left(f_{SC}^{-1}(\log(S)) - j\frac{h_r}{2} \right) + j\pi} \tag{6}$$

where h_r and w_r are the height and width of rectangle since the

SC mapping can transform the rectangle to polygon. The inner and outer radii (R_r and R_s) of slotted air-gap in S domain is conformally mapped to the radius $r_{\psi r}$ and $r_{\psi s}$ in Ψ domain. SC mapping is expressed as [19]

$$f_{SC}(W) = A_0 \int \prod_{k=1}^{n-1} (W - w_k)^{-\frac{\beta_k}{\pi}} dW + C_0 \tag{7}$$

Hence, the position (r_ψ, α_ψ) in the polar coordinate of Ψ domain is expressed as the Fourier series of the position (r_S, α_S) in the S domain using (6)-(7).

$$r_\psi = \sum_{k_i} \sum_{k_j} a_{rijl} \cos(k_i(w_r t + \alpha_j) + k_l \frac{2\pi}{h_m} r + \theta_{rijl})$$
$$\alpha_\psi = \sum_{k_i} \sum_{k_j} a_{\alpha ijl} \cos(k_i(w_r t + \alpha_j) + k_l \frac{2\pi}{h_m} r + \theta_{\alpha ijl}) \tag{8}$$

where w_r is the rotational speed of SPM motor. α_j represents initial position. a_{rijl}, θ_{rijl}, $a_{\alpha ijl}$, and $\theta_{\alpha ijl}$ can be calculated using (6)-(7). According to the superposition principle, the total magnetic vector potential of PM $A_z(r_{SPM}, \alpha_{SPM})$ is regarded as the sum of magnetic vector potential produced by the PM equivalent current, winding current and equivalent current of iron nonlinearity using (4), (5), and (8). Fig. 2 shows the position of the PM and the equivalent current in the conformal mapping. The winding current and equivalent current of iron nonlinearity will produce the time-varying magnetic field in the PM due to the synchronous changes of the PM position and the current value. Besides, although the relative positions of PM equivalent current and PM region are unchanged in the S domain, it will result in different relative positions in the Ψ domain due to the deformation of PM in the conformal mapping when considering slotting effect (see the green dotted line in Fig.2). Hence, the proposed model can give the mathematical explanation about the open-circuit magnet loss in the slotted SPM motor based on the theory of conformal mapping.
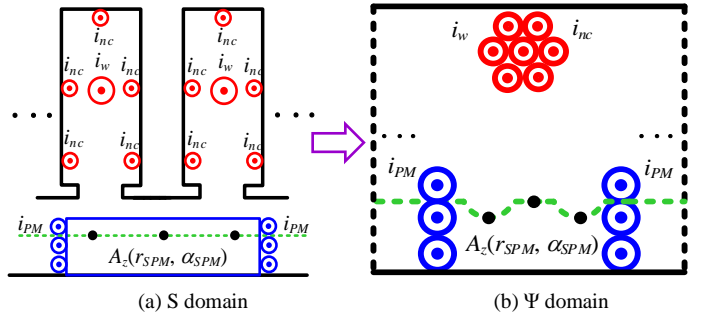

(a) S domain   (b) Ψ domain

Fig. 2 The conformal mapping of the equivalent current and the position of PM region in the PMSM.

The radial and circumferential flux density in the magnet region of SPM motor can be expressed as

$$B_{rS} = \frac{1}{r} \frac{\partial A_z(r_S, \alpha_S)}{\partial \alpha}$$
$$B_{\alpha S} = -\frac{\partial A_z(r_S, \alpha_S)}{\partial r} \tag{9}$$

III. MAGNET LOSS CALCULATION

Based on the nonlinear analytical solution of PM region, the eddy current in the magnet is calculated using

$$J_{eddy}(t) = -\sigma \frac{\partial A_z(r_s, \alpha_s)}{\partial t} + C_{PM}(t)$$

$$= \sum_{k=0}^{\infty} J_{ek} \cos(2\pi k f_0 t + \alpha_{ek}) \tag{10}$$

where f_0 is the fundamental frequency. σ is the magnet conductivity. J_{ek} and α_{ek} are the amplitude and phase of kth temporal order eddy current harmonic. The total eddy current in each piece of PM should be equal to zero. Therefore, $C_{PM}(t)$ can be obtained using

$$C_{PM}(t) = \frac{2\int_{\alpha_{sPM1}}^{\alpha_{sPM2}} \int_{r_{sPM1}}^{r_{sPM2}} \sigma \frac{\partial A_z(r_s, \alpha_s)}{\partial t} r dr d\alpha}{(\alpha_{sPM2} - \alpha_{sPM1})(r_{sPM2}^2 - r_{sPM1}^2)} \tag{11}$$

where the time derivative of vector magnetic potential is shown in (12) at the bottom of next page. Then the instantaneous and average magnet loss in each piece of magnet can be obtained as

$$p_e = \frac{l_e}{\sigma} \int_{\alpha_{sPM1}}^{\alpha_{sPM2}} \int_{r_{sPM1}}^{r_{sPM2}} J_{eddy}^2 r dr d\alpha$$

$$= \sum_{k=0}^{\infty} p_{ek} \left[1 + \cos(4\pi k f_0 t + 2\alpha_{ek}) \right] \tag{13}$$

$$P_{ave} = f_0 \int_0^{1/f_0} p_e dt = \sum_{k=0}^{\infty} p_{ek} \tag{14}$$

where l_e represents the effective length.

IV. FINITE-ELEMENT VALIDATION

An 8-pole/9-slot and a 10-pole/12-slot SPM motors are designed and analyzed using the NAM and Ansys Maxwell to show the accuracy of magnet loss calculation, Fig. 3. The geometric parameters are listed in TABLE I. It can be found that the iron saturation occurs in the tooth body and stator yoke. Therefore, the iron saturation cannot be neglected in the calculation of magnet loss.
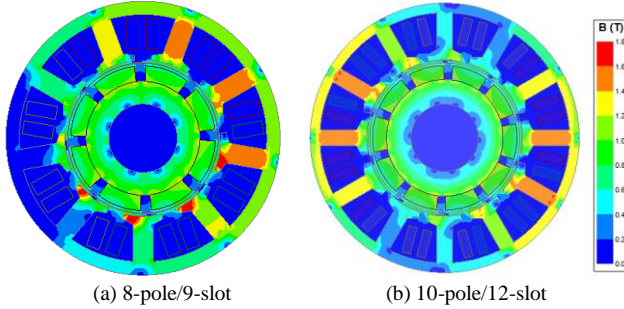

(a) 8-pole/9-slot   (b) 10-pole/12-slot
Fig. 3 The flux density distribution of SPM motors.

TABLE I
THE GEOMETRIC PARAMETERS OF SPM MOTOR (UNIT: MM)

Parameter	8-pole/9-slot	10-pole/12-slot
Stator outer diameter	80	
Rotor inner diameter	20	
Axial length	80	
Air-gap length	1.7	
Pole-arc to pole-pitch ratio	0.8	
Tooth body height	10.8	10.8
Stator yoke height	3.9	2.9
Stator inner diameter	45.6	23.2
Slot opening	5	2.5
PM height	4.5	4.2

Figs. 4-5 shows the comparison of magnetic field prediction in PM region at rated load. The proposed model can accurately obtain the flux density in PM region, which is the key for accurate prediction of magnet loss.
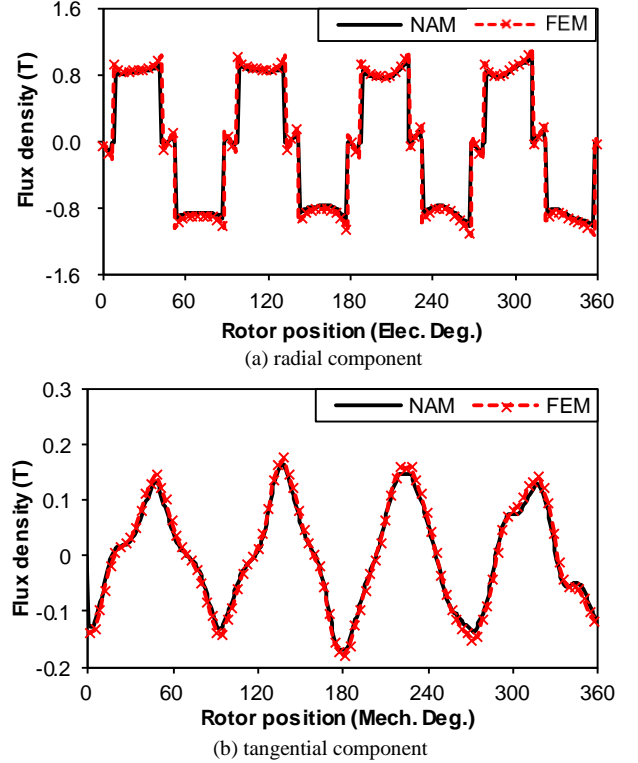

(a) radial component

(b) tangential component
Fig. 4 The air-gap field along the middle PM for 8-pole/9-slot motor at 40A.
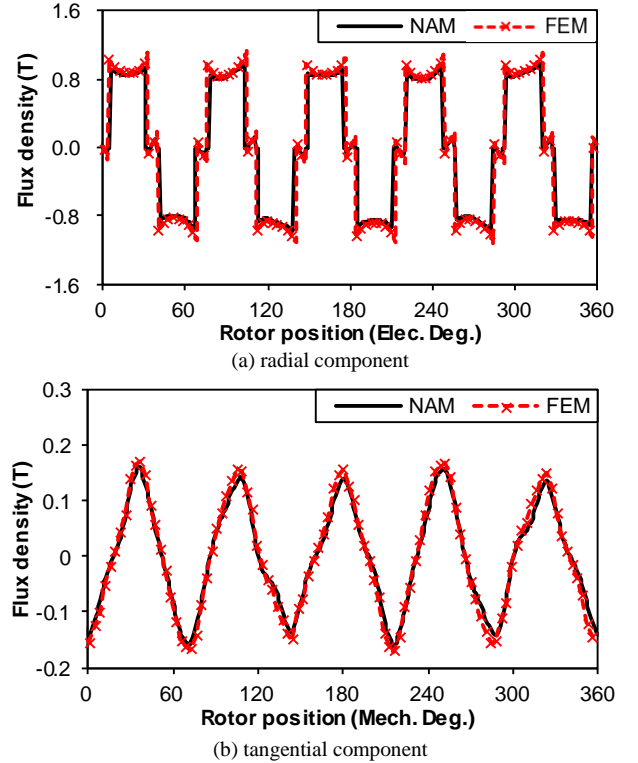

(a) radial component

(b) tangential component
Fig. 5 The air-gap field along the middle PM for 10-pole/12-slot motor at 30A.

In Figs. 6-7, the average magnet loss distribution in single PM region is calculated for both motors at 12000rpm. The magnet loss is larger at both sides of PM than that in the central

PM. It means that the eddy current mainly exists at the two sides of PM, to which the motor designers should pay more attention for the reduction of magnet loss.
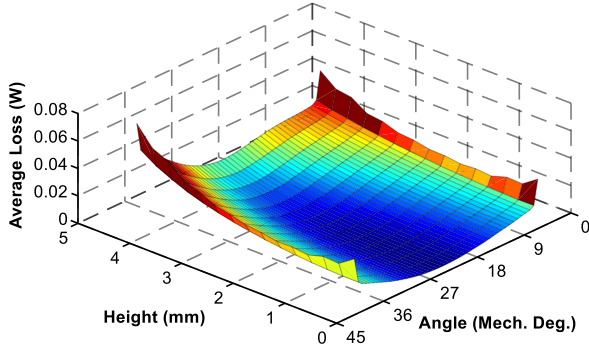

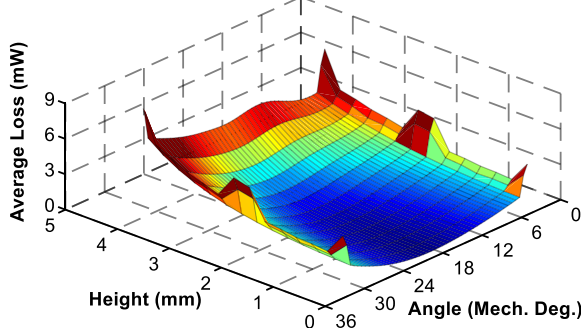Fig. 6 The average magnet loss distribution for 8-pole/9-slot motor at 40A.

Fig. 7 The average magnet loss distribution for 10-pole/12-slot motor at 30A.

Figs. 8-9 give the temporal magnet loss harmonic amplitude in the small pieces of magnet, whose radii are $(R_r+h_m/2)$ and angular positions are varied. There are large components of magnet loss harmonic at both sides of PM, especially for high temporal order harmonic. It also illustrates that the magnet loss is mainly produced at two sides of PM.
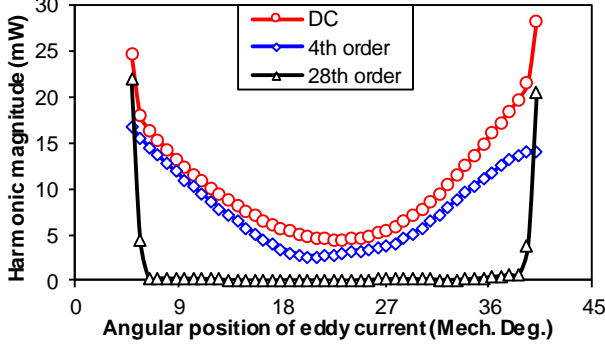

Fig. 8 The major component of temporal magnet loss harmonic at $(R_r+h_m/2)$ in one magnet for 8-pole/9-slot motor.
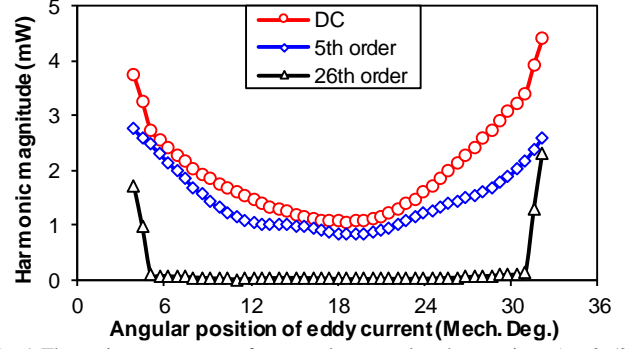

Fig. 9 The major component of temporal magnet loss harmonic at $(R_r+h_m/2)$ in one magnet for 10-pole/12-slot motor.

For both motors, their magnet loss increases significantly as the rotational speed becomes higher at rated load, Figs. 10-11. The magnet loss using NAM matches well with that using nonlinear FEM. If the equivalent current of iron nonlinear is neglected, the prediction of linear analytical model (LAN) can agree well with linear FEM results with infinitely permeable iron. Comparing the linear prediction and nonlinear predictions, the iron nonlinearity can also decrease the magnet loss.
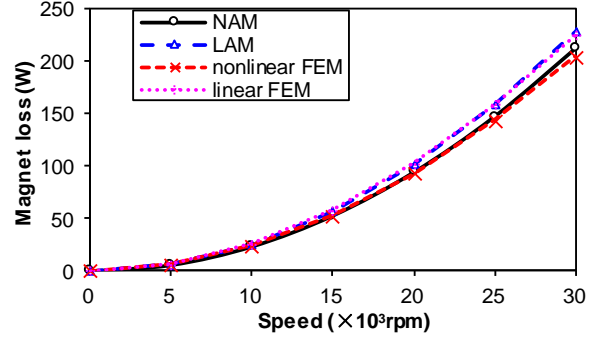

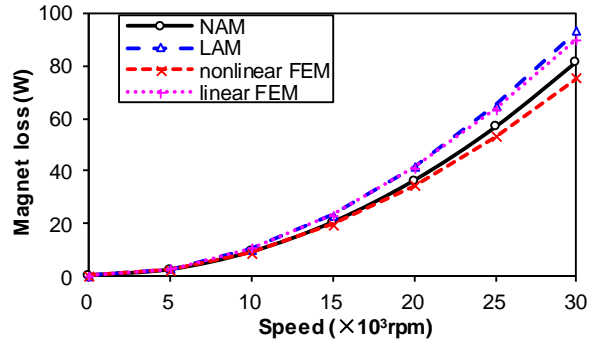Fig. 10 The varication of magnet loss to speed for 8-pole/9-slot motor.

Fig. 11 The varication of magnet loss to speed for 10-pole/12-slot motor.

$$
\begin{aligned}
\frac{\partial A_z}{\partial t} = \frac{\mu_0 i_c}{2\pi} \Bigg\{ &\sum_{k=1}^{+\infty} \frac{2r_{\psi PM} r_{\psi PM}{'} + 2r_{\psi c} r_{\psi c}{'} - 2\left(r_{\psi c} r_{\psi PM}{'} + r_{\psi PM} r_{\psi c}{'}\right)\cos(\alpha_{\psi PM} - \alpha_{\psi c}) + 2r_{\psi PM} r_{\psi c}\left(\alpha_{\psi PM}{'} - \alpha_{\psi c}{'}\right)\sin(\alpha_{\psi PM} - \alpha_{\psi c})}{r_{\psi PM}^2 + r_{\psi c}^2 - 2r_{\psi PM} r_{\psi c}\cos(\alpha_{\psi PM} - \alpha_{\psi c})} \\
&+ \frac{r_{\psi r}^{2k}\left[-r_{\psi PM}^{k-1} r_{\psi s}^{-k}\left(r_{\psi c}^{2k} r_{\psi r}^{-2k} + 1\right) + r_{\psi PM}^{-k-1} r_{\psi s}^{k}\left(r_{\psi s}^{-2k} r_{\psi c}^{2k} + 1\right)\right]r{'}_{\psi PM} - 2r_{\psi r}^{2k} r_{\psi s}^{-k} r_{\psi c}^{2k-1}\left[r_{\psi PM}^{k} r_{\psi r}^{-2k} + r_{\psi PM}^{-k}\right]r_{\psi c}{'}}{\left(r_{\psi s}^{2k} - r_{\psi r}^{2k}\right)} \cos\left[k\left(\alpha_{\psi PM} - \alpha_{\psi c}\right)\right] \\
&+ \frac{r_{\psi r}^{2k}\left[r_{\psi PM}^{k} r_{\psi s}^{-k}\left(r_{\psi c}^{2k} r_{\psi r}^{-2k} + 1\right) + r_{\psi PM}^{-k} r_{\psi s}^{k}\left(r_{\psi s}^{-2k} r_{\psi c}^{2k} + 1\right)\right]}{\left(r_{\psi s}^{2k} - r_{\psi r}^{2k}\right)}\left[\alpha_{\psi PM}{'}\sin\left[k\left(\alpha_{\psi PM} - \alpha_{\psi c}\right)\right] - \alpha_{\psi c}{'}\sin\left[k\left(\alpha_{\psi PM} - \alpha_{\psi c}\right)\right]\right]\Bigg\} \\
&= \sum_i \sum_l b_{ijl} \cos\left[m_i(w_r t + \alpha_j) + m_l \frac{2\pi}{h_m} r + \theta_{rijl}\right]
\end{aligned}
\tag{12}
$$

Similarly, the magnet loss is greatly affected by the load condition for both motors, Figs. 12-13. The NAM still achieves high accuracy compared with nonlinear FEM results. If the iron nonlinearity is neglected, the analytical model will significantly overestimate the magnet loss for both motors.
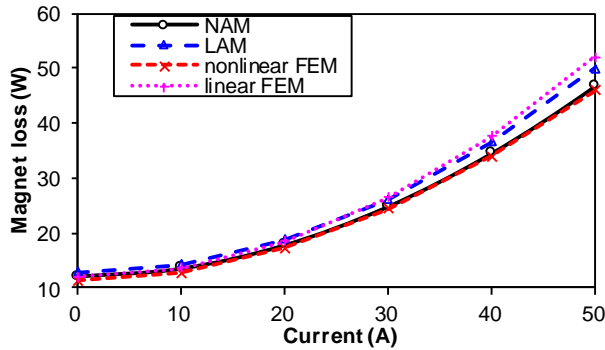

Fig. 12 The varication of magnet loss to load current for 8-pole/9-slot motor at 12000rpm.
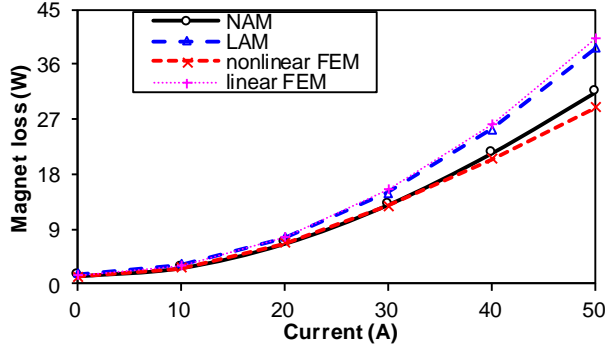

Fig. 13 The varication of magnet loss to load current for 10-pole/12-slot motor at 12000rpm.

As for calculation time, the commercial software Ansys Maxwell based on FEM consumes 547s and 425s for 8-pole/9-slot and 10-pole/12-slot motors, respectively. Comparatively, the NAM takes 181s and 162s to predict the magnet loss for both motors. Therefore, the proposed analytical model will save nearly 2/3 of the computational resource using FEM.

V. CONCLUSION

In this paper, the NAM is proposed to predict the magnet loss for SPM motor considering both slotting effect and nonlinearity effect. The vector magnetic potential of PM region is obtained using the supposition principal of total equivalent current including PM, winding current, and iron nonlinearity. The equivalent current of iron nonlinearity is calculated from the improved magnetic circuit model, where the air reluctance is replaced by the air flux source. According to the analytical solution of vector magnetic potential in PMs, the magnet loss is mainly located at both sides of PMs and it is also decreased due to iron nonlinearity. Both high accuracy and high efficiency of NAM is validated by the FEM.

ACKNOWLEDGMENT

REFERENCES

[1] Z. Q. Zhu and D. Howe, "Electrical machines and drives for electric, hybrid, and fuel cell vehicles," *Proc. IEEE,* vol. 95, no. 4, pp. 746–765, Apr. 2007

[2] K. Yamazaki, Y. Fukushima, and M. Sato, "Loss analysis of permanent-magnet motors with concentrated windings-variation of magnet eddy-current loss due to stator and rotor shapes," *IEEE Trans. Ind. App.*, vol. 45, no. 4, pp. 1334–1342, Jul. 2009.

[3] Z. Q. Zhu and D. Howe, "Instantaneous magnetic field distribution in brushless permanent magnet DC motors. II. Armature-reaction field," *IEEE Trans. Magn.,* vol. 29, no. 1, pp. 136-142, Jan. 1993.

[4] Z. Q. Zhu and D. Howe, "Instantaneous magnetic field distribution in brushless permanent magnet dc motors. Part III: Effect of stator slotting", *IEEE Trans. Magn.,* vol. 29, no. 1, pp. 143-151, Jan. 1993.

[5] D. Zarko, D. Ban and T. A. Lipo, "Analytical calculation of magnetic field distribution in the slotted air gap of a surface permanent-magnet motor using complex relative air-gap permeance", *IEEE Trans. Magn.,* vol. 42, no. 7, pp. 1828-1837, Jul. 2006.

[6] H. Toda, Zhenping Xia, Jiabin Wang, K. Atallah and D. Howe, "Rotor eddy-current loss in permanent magnet brushless machines," *IEEE Trans. Magn.,* vol. 40, no. 4, pp. 2104-2106, July 2004.

[7] Z. Q. Zhu, K. Ng, N. Schofield and D. Howe, "Analytical prediction of rotor eddy current loss in brushless machines equipped with surface-mounted permanent magnets. I. Magnetostatic field model," *Proc. Int. Conf. Electr. Machines and Syst.,* pp. 806-809, vol. 2, 2001.

[8] Tim C. O'Connell and P.T. Krein, "A Schwarz-Christoffel-based analytical method for electric machine field analysis," *IEEE Trans. Energy Convers.,* vol. 24, no. 3, pp. 565-577, 2009.

[9] K. Ramakrishnan, D. Zarko, A. Hanic, and G. Mastinu, "Improved method for field analysis of surface permanent magnet machines using Schwarz–Christoffel transformation," *IET Electr. Power App.,* vol. 11, no. 6, pp. 1067-1075, Jun 2017.

[10] L. J. Wu, Z. Q. Zhu, D. Staton, M. Popescu, and D. Hawkins, "An improved subdomain model for predicting magnetic field of surface-mounted permanent magnet machines accounting for tooth-tips," *IEEE Trans. Magn.*, vol. 47, no. 6, pp. 1693–1704, Jun. 2011.

[11] L. J. Wu, Z. Q. Zhu, D. A. Staton, M. Popescu, and D. Hawkins, "Comparison of analytical models of cogging torque in surface-mounted pm machines," *IEEE Trans. Ind. Electron.*, vol. 59, no. 6, pp. 2414–2425, Jun. 2012.

[12] N. Chiodetto, N. Bianchi, and L. Alberti, "Improved analytical estimation of rotor losses in high-speed surface-mounted PM synchronous machines," *IEEE Trans. Ind. App.*, vol. 53, no. 4, pp. 3548–3556, Jul. 2017.

[13] P. D. Pfister, X. Yin, and Y. Fang, "Slotted permanent-magnet machines: general analytical model of magnetic fields, torque, eddy currents, and permanent-magnet power losses including the diffusion effect," *IEEE Trans. Magn.*, vol. 52, no. 5, pp. 1–13, May 2016.

[14] L. J. Wu, Z. K. Li, X. Y. Huang, Y. L. Zhong, Y. T. Fang, and Z. Q. Zhu, "A hybrid field model for open-circuit field prediction in surface-mounted PM machines considering saturation," *IEEE Trans. Magn.*, vol. 54, no. 6, pp. 1-12, June 2018.

[15] L. J. Wu, Z. Li, D. Wang, H. Yin, X. Huang, and Z. Q. Zhu, "On-load field prediction of surface-mounted pm machines considering nonlinearity based on hybrid field model," *IEEE Trans. Magn.*, vol. 55, no. 3, pp. 1–11, Mar. 2019.

[16] A. Hanic, D. Zarko, and Z. Hanic, "A novel method for no-load magnetic field analysis of saturated surface permanent-magnet machines using conformal mapping and magnetic equivalent circuits," *IEEE Trans. Energy Convers.*, vol. 31, no. 2, pp. 740-749, Jun. 2016.

[17] A. Hanic, D. Zarko, D. Kuhinek, and Z. Hanic, "On-Load analysis of saturated surface permanent magnet machines using conformal mapping and magnetic equivalent circuits," *IEEE Trans. Energy Convers.*, vol. 33, no. 3, pp. 915-924, Sept. 2018.

[18] B. Hague, "The principles of electromagnetism applied to electrical machines,", New York: Dover Publications, 1962.

[19] T. A. Driscoll, Schwarz-Christoffel Toolbox User's Guide: Version 2.3. Newark, DE, USA: Univ. Delaware, 2005.